Measurement of quasielastic and transfer excitation functions in ^{16}O, ^{19}F+^{232}Th reactions

Shrabani Sinha and R. Varma
Department of Physics, Indian Institute of Technology, Bombay, Powai, Mumbai 400 076, India

R. K. Choudhury, B. K. Nayak, A. Saxena, R. G. Thomas, and B. V. Dinesh
Nuclear Physics Division, Bhabha Atomic Research Centre, Mumbai 400 085, India

(Received 9 July 1999; published 17 February 2000)

Quasielastic (QE) and transfer excitation function measurements have been carried out for the ^{16}O, ^{19}F + ^{232}Th systems at $\theta_{lab}=170°$ over a wide energy range above and below the Coulomb barrier. The data were analyzed to obtain the representation of fusion barrier distributions as well as the mean square compound nuclear spin values ($\langle I^2\rangle$), which are found to compare well with the results of the standard fusion model (CCDEF) calculations. Further, the back-angle transfer cross-section data as a function of the bombarding energy were transformed to give the transfer probabilities as a function of the distance of closest approach for $1p$, $2p$, 1α, and $1p1\alpha$ transfer channels. The experimental ''slope parameters'' derived from these data were compared with the predictions of the semiclassical model calculations. It is found that the results for single nucleon or single cluster transfers are well explained by the semiclassical model, whereas for multinucleon or cluster transfers, the calculations underpredict the transfer probabilities.

PACS number(s): 25.70.Bc, 25.70.Hi, 25.70.Jj

I. INTRODUCTION

In recent years, the study of heavy ion reactions at near and below barrier energies has received a lot of attention. This is primarily because of the large enhancements observed in the fusion cross sections relative to that expected from the one dimensional barrier penetration model calculations at sub-barrier energies. In the simplest picture, the sub-barrier fusion of two interacting nuclei is due to the quantum mechanical tunneling through an effective potential barrier arising from Coulomb, nuclear and centrifugal interactions between the two nuclei [1]. The enhancement in fusion cross sections at energies below the barrier has been explained as being due to coupling between the relative motion and the internal degrees of freedom of the colliding nuclei, such as static deformations, collective vibrations, inelastic excitations and nucleon transfer, etc. [2]. These channel couplings also lead to a distribution of the fusion potential barriers and are expected to influence both fusion and quasielastic reactions at energies close to the Coulomb barrier. It has been shown that the representation of fusion barrier distributions can be extracted directly from the fusion excitation function measurements [3] by taking the second derivative of the product of energy E and fusion cross section $\sigma^{fus}(E)$ with respect to the center-of-mass energy of the projectile ($D^{fus}(E)=(1/\pi R^2)(d^2/dE^2)[E\sigma^{fus}(E)]$). The experimentally derived barrier distributions, for various systems, have provided valuable information to study the effect of the structure of target and projectile nuclei and the coupling of various excited states and transfer channels to the fusion process.

In heavy ion reactions, the dynamics of elastic, inelastic, transfer and fusion reactions are interrelated. It has been shown that the information on the fusion barrier distribution can also be obtained from the quasielastic (QE) excitation function measurements at backward angles [4]. The quasielastic scattering includes elastic as well as inelastic and transfer channels.

In an earlier work [5], we have reported the measurement of the representation of fusion barrier distribution and spin distribution via the quasielastic scattering at energies near and below the Coulomb barrier. In the present work, we have extended these studies to ^{16}O, ^{19}F+^{232}Th systems to determine the fusion barrier distributions and spin distributions from the QE excitation function measurements at backward angles. A systematic study of the fusion barrier distributions in these different systems is useful to investigate the role of channel couplings and projectile structure in governing the fusion dynamics in heavy fissile systems.

We have also investigated in detail the cross sections of various transfer channels in the ^{16}O, ^{19}F+^{232}Th reactions at below and above barrier energies. The study of transfer reactions is expected to provide valuable insight into the reaction mechanism of these direct and semidirect processes. One of the most important problems in these studies is to identify the relevant degrees of freedom that correctly describe the single and multinucleon transfer processes. More specifically, it is important to understand if single nucleon transfer modes would describe the more complex multinucleon transfer processes or one needs to invoke complex mechanisms such as cluster and correlated nucleon transfers to describe these processes [6].

It has been seen from earlier studies that the structural properties of the two nuclei could influence the transfer probabilities (P_{tr}) in different transfer channels [7–9]. The transfer cross sections are primarily governed by the tunneling probability for the particle which is to be transferred from the projectile to the target or vice versa. At reaction energies near the Coulomb barrier, the semiclassical model predicts that P_{tr} should fall off exponentially with the distance of closest approach D. P_{tr} is given by the relation $P_{tr} \propto \exp[-2\alpha D]$. The slope parameter ($\alpha$) is given by $\sqrt{2\mu E_b}/\hbar$, where μ is the reduced mass of the transferred

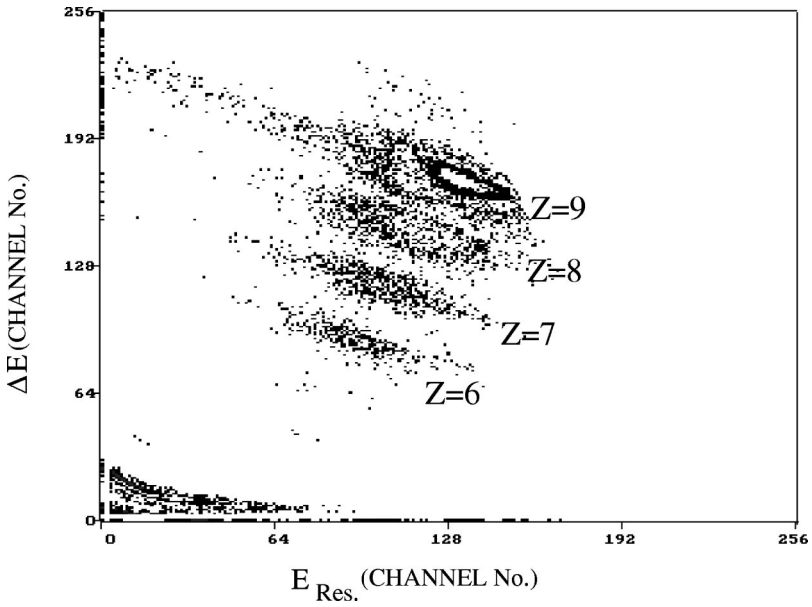

FIG. 1. The ΔE–E_{Res} correlation plots at $E_{\mathrm{lab}}=99$ MeV for $^{19}\mathrm{F}+^{232}\mathrm{Th}$ system.

nucleon and the nucleus to which it is transferred and E_b is the binding energy of the transferred nucleons inside the projectile. The two nucleon transfer probability, with this definition of P_{tr} should be approximately the square of the probability for one-nucleon transfer, regardless of whether the process is sequential or correlated, i.e., $P_2=(P_1)^2\propto\exp[2(-2\alpha D)]$. However, in many experiments, usually at above barrier energies, one finds that the slope parameter for two-nucleon transfer is greater than twice that for one-nucleon transfer [10]. This large departure of the two-nucleon slope factors α_{2n},α_{2p} from the expected value $\alpha_{2n},\alpha_{2p}\approx 2\alpha_{1n},2\alpha_{1p}$ has come to be known as the ''slope anomaly.'' In the above, D is usually determined from the Coulomb deflection functions of the projectile as a function of the scattering angle, and the ''slope anomaly'' observed for one- and two-nucleon transfer reactions at large internuclear distances has been explained to be due to contributions to the transfer probability from the Coulomb and nuclear branches of the classical deflection function [11]. In the present work, we have measured the transfer cross sections at a fixed backward angle with projectile energies varying from above barrier to sub-barrier energies. The distance of closest approach D, in this case is varied by varying the bombarding energy in the sub-barrier region and can be calculated from the Coulomb trajectories for near head on collisions corresponding to $l\approx 0\hbar$. The present results on the transfer probabilities as a function of D, therefore, can provide an alternate way to determine the ''slope parameters'' for comparison with the semiclassical model calculations.

The paper is organized as follows. In Sec. II we describe the experimental setup and data analysis procedure. Section III gives the discussion of the experimental results on the fusion barrier and spin distributions as obtained from the quasielastic excitation functions. In Sec. IV, we discuss the results on the transfer probabilities in various transfer reaction channels on the basis of the semiclassical model calculations. Section V contains a summary and conclusions of the present investigations.

II. EXPERIMENTAL DETAILS AND DATA ANALYSIS

The experiments were carried out using the $^{16}\mathrm{O}$ and $^{19}\mathrm{F}$ beams from the 14 MV BARC-TIFR pelletron accelerator facility in Mumbai. A self-supporting $^{232}\mathrm{Th}$ target of 1.8 mg/cm^2 thickness was used in the experiment. The measurements were carried out over the bombarding energy range of $E_{\mathrm{lab}}=73$–99 MeV for the $^{16}\mathrm{O}$ projectile and $E_{\mathrm{lab}}=83$–109 MeV for the $^{19}\mathrm{F}$ projectile in steps of 2 MeV for each projectile. A silicon surface barrier detector telescope [$\Delta E(17\ \mu)$–$E(1.0\ \mathrm{mm})$] was kept at $\theta_{\mathrm{lab}}=170°$ to detect the elastically scattered particle and projectilelike transfer products. Another silicon surface barrier detector, mounted at an angle of $\theta_{\mathrm{lab}}=20°$, was used to measure Rutherford scattering events for relative normalization between different runs and for the determination of the absolute cross sections. The energy loss in half the target thickness for $^{16}\mathrm{O}$ beam is between $\sim$1.1–1.5 MeV and for $^{19}\mathrm{F}$ beam, the energy loss is between $\sim$1.6–1.9 MeV over the full range of bombarding energies. In all the experimental results discussed below, the energy loss corrections have been incorporated.

Figure 1 shows a typical two dimensional plot of ΔE–E_{Res} from the detector telescope, showing elastic and various transfer channels for $^{19}\mathrm{F}+^{232}\mathrm{Th}$ reaction at $E_{\mathrm{lab}}=99$ MeV. The various outgoing reaction product charges (Z) are clearly identified in the experiment. The energy calibration of the telescope was done from the observed peak positions of the elastic peak at different bombarding energies in both the reactions. The calibration for both ΔE and E_{Res} detectors was found to be quite linear in the entire energy range. The mass and charge identification of the different isotopes was carried out using the multiplier algorithm [12] $\mathrm{PIO}=\Delta E\times(E_{\mathrm{Res}}+k_1\times\Delta E+k_2)$ where ''k_1'' and ''k_2'' are constants and PIO is the particle identification operator. It was observed that the best mass and charge separation for all the elements is achieved with a value of $k_1=2.7$ and $k_2=-10.0$. One of the typical particle identification spectra obtained for the $^{19}\mathrm{F}+^{232}\mathrm{Th}$ reaction at $E_{\mathrm{lab}}=99$ MeV is

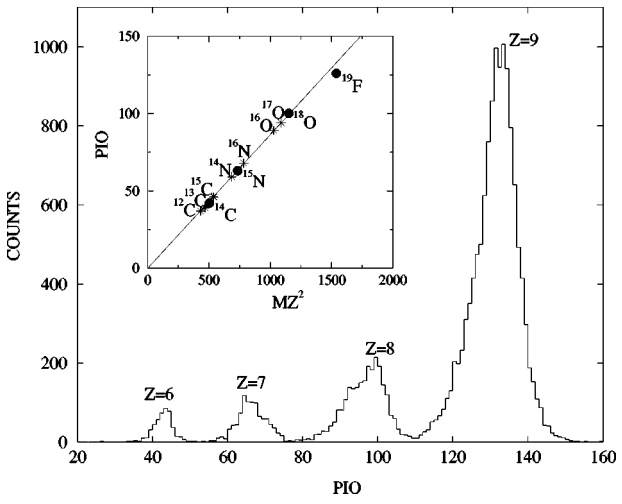

FIG. 2. Particle identification (PI) spectrum at $E_{\mathrm{lab}}=99$ MeV for $^{19}\mathrm{F}+^{232}\mathrm{Th}$ at $\theta_{\mathrm{lab}}=170°$. The inset in the figure for PI spectra is a typical calibration curve where the particle identification operator (PIO) is plotted as a function of MZ^2.

shown in Fig. 2 along with a calibration plot of PIO (particle identification operator) vs MZ^2 for all possible isotopes of transfer products. A linear relation between the PIO and MZ^2 product for the dominant isotopes (shown as solid circles in the inset) was observed which enabled us to locate the peak positions of all the possible isotopes in the particle identification spectra (as shown by the stars in the plot in the inset). This linear relationship gave us reasonable confidence in unfolding the particle identification spectra. The isotopic yields of different transfer products were obtained by deconvoluting the PIO spectra with multiple Gaussian peak fitting as is shown in Fig. 3. The σ of the PIO as obtained from these fits is seen to be less than 0.5 a.m.u. over the full range of the isotopes covered in the experiment, corresponding to the FWHM of around 1 mass unit. In the deconvolution procedure, the peak positions were fixed at values given by the above calibration, the area and FWHM were adjusted to give the best fit to the data with minimum χ^2 values for each isotope.

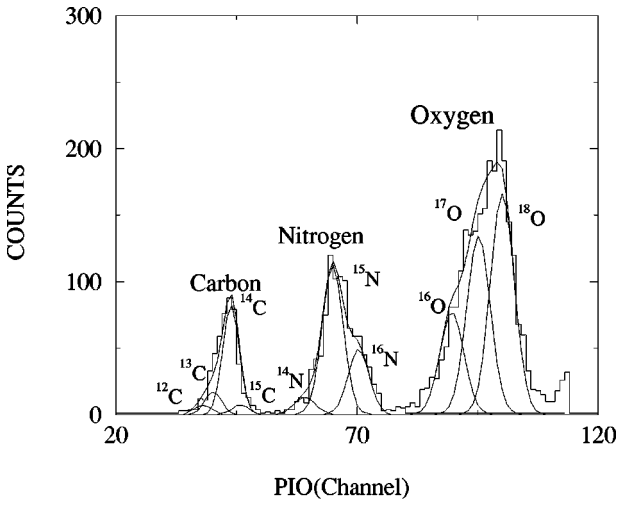

FIG. 3. The various isotopic yields of the outgoing transfer reaction products obtained by Gaussian deconvolution of the mass distribution of different elements $Z=8$, $Z=7$, and $Z=6$ at 99 MeV for $^{19}\mathrm{F}+^{232}\mathrm{Th}$ reaction at $\theta_{\mathrm{lab}}=170°$ are labeled.

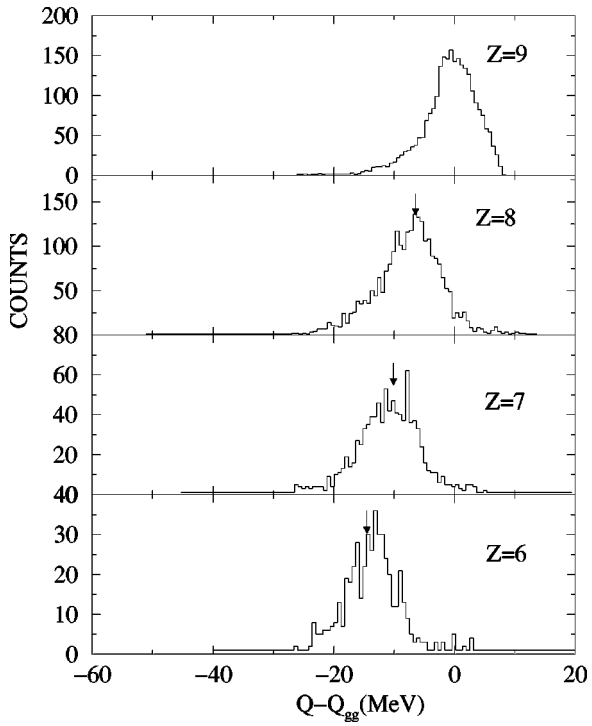

FIG. 4. Q-value spectra of $Z=9$, 8, 7, and 6 projectilelike fragments in the $^{19}\mathrm{F}+^{232}\mathrm{Th}$ reaction at $\theta_{\mathrm{lab}}=170°$ for bombarding energy $E_{\mathrm{lab}}=99$ MeV. The arrows indicate the corresponding Q_{opt} values.

In case of $^{19}\mathrm{F}$ induced reaction, the dominant transfer products are seen to be $^{18}\mathrm{O}$, $^{15}\mathrm{N}$, and $^{14}\mathrm{C}$ corresponding to $1p$, 1α, and $1\alpha 1p$ transfers, whereas for $^{16}\mathrm{O}$ induced reaction, the dominant products are $^{15}\mathrm{N}$, $^{12}\mathrm{C}$, and $^{14}\mathrm{C}$ corresponding to $1p$, 1α, and $2p$ transfers, respectively. The two body character of the transfer products can be seen by examining the energetics of the reaction, as evidenced by the energy spectra of the reaction products. The observed energies of the products were converted to the reaction Q values by assuming two body kinematics. Figure 4 shows the energy spectra corresponding to the most probable isotopes of $Z=9$, 8, 7, and 6 products plotted in terms of the Q value in the $^{19}\mathrm{F}+^{232}\mathrm{Th}$ reaction at $E_{\mathrm{lab}}=99$ MeV. The observed energies of the products were converted to the reaction Q values by assuming two body kinematics. The energy spectra are found to peak at energies corresponding to the Q_{opt} values $[Q_{\mathrm{opt}}=E_{\mathrm{c.m.}}((z_f Z_f/z_i Z_i)-1)$, where i and f refer to the incoming and outgoing channels, respectively] as shown by arrows in Fig. 4. In Fig. 4, the spectra are shown as a function of Q-Q_{gg}, which gives directly the excitation energy of the transfer partners (Q_{gg} is the ground state Q value for the transfer channel). It is seen that the excitation energy spectra move up by about 5–6 MeV for one unit increase in the charge transfer. In the semiclassical picture, at Q_{opt} there is maximum overlap of the Coulomb wave functions in the initial and final channels giving rise to the maximum in the

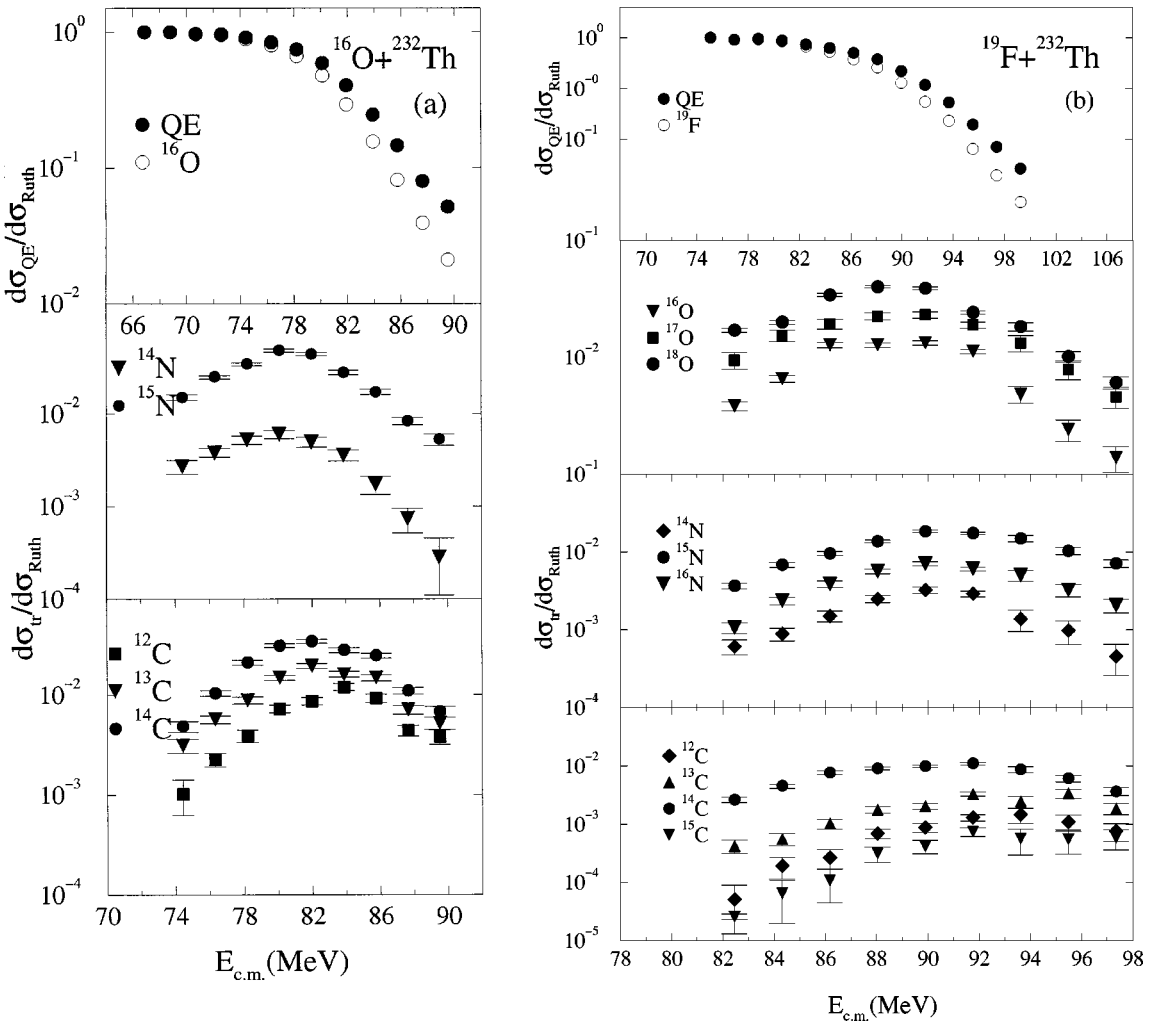

FIG. 5. (a) Quasielastic and transfer excitation functions for ^{16}O+^{232}Th reactions at $\theta_{lab}=170°$. (b) Quasielastic and transfer excitation functions for ^{19}F+^{232}Th reactions at $\theta_{lab}=170°$.

transfer yields at that energy. The agreement between the average energy of the transfer product and the Q_{opt} implies that the semiclassical picture seems to hold good for the average behavior of the most probable transfer channels. The energy integrated cross sections of the quasielastic scattering and transfer channels normalized to the Rutherford scattering cross sections for both ^{16}O, ^{19}F+^{232}Th reactions as measured at the fixed backward angle of $\theta_{lab}=170°$ are shown in Figs. 5(a) and 5(b). The quasielastic cross sections as shown by the solid circles in the top part of the figures correspond to the sum of elastic, inelastic and transfer channels whereas the hollow circles correspond to only the elastic scattering channel. It is seen that the elastic scattering cross section at backward angles drops rapidly above the fusion barrier, whereas the transfer channels have a bell-shaped behavior with broad maximum around the barrier energy. As will be shown later in Sec. IV, the below barrier data for the different transfer channels were used to study the transfer probabilities for both the systems as a function of the distance of closest approach obtained by using the Coulomb trajectories.

III. FUSION BARRIER AND SPIN DISTRIBUTIONS

A. Fusion barrier distribution

The representation of fusion barrier distributions $D^{qe}(E)$ for ^{16}O, ^{19}F+^{232}Th systems has been extracted from the quasielastic excitation functions measured at $\theta_{lab}=170°$ in a manner similar to that mentioned in Ref. [5]. The results of $D^{qe}(E,170°)$ were converted to that of $D^{qe}(E,180°)$ by reducing the centrifugal energy from the energy scale.

The results of the barrier distribution $D^{qe}(E)$ obtained from the present analysis for the ^{16}O and ^{19}F+^{232}Th systems along with the earlier results for ^{12}C+^{232}Th [5] are shown in Fig. 6. The fusion barrier distributions as calculated using the coupled channel fusion model CCDEF [13] which fits the experimental fission excitation function data [14] are also shown in Fig. 6. In the CCDEF calculations, the ground state deformations and inelastic excitations of the target nucleus ($\beta_2=0.22$ and $\beta_4=0.09$ with excitation energy 0.774 MeV) were used. For ^{19}F projectile, three excited states at 0.197, 1.346, and 1.554 MeV with $\beta_2=0.55$, $\beta_3=0.33$, and $\beta_4=0.22$ respectively were used. It is seen from Fig. 6 that the

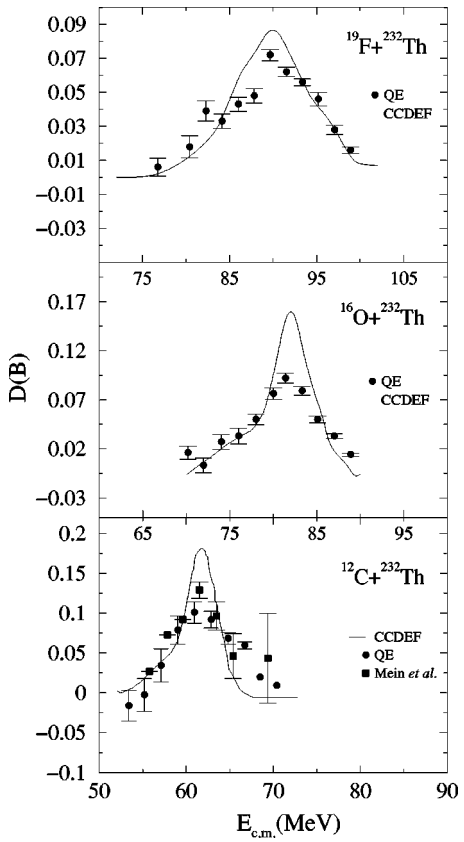

FIG. 6. The fusion barrier distribution obtained from quasielastic scattering measurements along with the barrier distribution obtained from the CCDEF for ^{12}C, ^{16}O, and ^{19}F+^{232}Th reactions. Also shown in the figure is the fusion barrier distribution obtained from fusion excitation measurement of Ref. [23] for ^{12}C+^{232}Th.

predictions of the coupled channel fusion model qualitatively agree with the experimentally determined fusion barrier distributions obtained from the quasielastic excitation functions. The barrier widths and barrier positions of the three systems as obtained from the experimentally measured barrier distributions for all the three systems are summarized in Table I. It is clear that the width of the experimental barrier distribution increases with increasing charge and mass of the projectile. One can understand the origin of the width of the barrier distribution by a simple geometrical argument valid for deformed targets. As mentioned earlier, the structure of the interacting nuclei strongly influences the cross section for fusion which in turn affects the barrier distribution. Geometrically, the Coulomb barrier is lower when the projectile approaches the tips of a deformed target nucleus and is higher when it approaches the equator of the target nucleus as compared to the case when the target nucleus is spherical. An average over all possible orientations of the target and the projectile nuclei produces a distribution of barrier heights, some lower and some higher than the spherical case. One can, therefore, write the total cross section as

$$\sigma^{\mathrm{fus}} = \int_0^{\pi/2} \sigma^{\mathrm{fus}}(E,\theta)\sin\theta d\theta, \tag{1}$$

where the θ is the angle between symmetry axis and the point of interaction. Assuming classical description of the fusion process, the barrier distribution can be written as

$$D(B) = \frac{1}{\pi R^2}\frac{d^2(E\sigma)}{(dE^2)} = \sin\theta\frac{d\theta}{dB}. \tag{2}$$

$D(B)dB = \sin\theta d\theta$. For a deformed target nucleus with a sharp nuclear surface and a quadrupole deformation β_2, the barrier position and barrier height may be parametrized with the prescription given in Ref. [15] as described below. The radius parameter and barrier can be expressed as a function of angle θ, with respect to the symmetry axis as

$$R(\theta) \approx R_B + R_T\beta_2 Y_{20}(\theta,0) \tag{3}$$

and

$$B(\theta) \approx \frac{Z_1 Z_2 e^2}{4\pi\epsilon_0}\frac{1}{R_B + R_T\beta_2 Y_{20}(\theta,0)}. \tag{4}$$

One, therefore, obtains the width of the barrier distribution as

$$\Delta B \approx \frac{3}{2}\sqrt{\frac{5}{4\pi}}\frac{Z_1 Z_2 e^2}{4\pi\epsilon}\frac{R_T}{R_B^2}\beta_2. \tag{5}$$

The barrier width is thus related to the product of the projectile and the target charges Z_1 and Z_2, average target radius R_T, average barrier radius R_B and deformation β_2. The barrier widths were calculated using Eq. (5) and are also tabulated in Table I. The calculated widths of the barrier distributions are larger than those extracted from the experimentally measured barrier distributions. Moreover, the experimental barrier widths seem to scale somewhat to a lesser extent with projectile charge than would be expected out of the above simple relationship.

B. Spin distributions

As discussed in the previous section the barrier distribution obtained from quasielastic scattering excitation function

TABLE I. Fusion barrier and optical model potential parameters.

	Barrier parameters (MeV)			ECIS parameters					
System	ΔB_{expt}	Positions	ΔB_{calc}	V(MeV)	W(MeV)	r_0 (fm)	a_0 (fm)	r_{i0} (fm)	a_{i0} (fm)
^{12}C+^{232}Th	11.83	60.95	11.6	40.0	10.0	1.1	0.8	1.4	0.19
^{16}O+^{232}Th	12.81	81.25	15.40	40.0	15.0	1.1	0.8	1.4	0.19
^{19}F+^{232}Th	15.61	89.8	17.21	40.0	35.0	1.1	0.8	1.4	0.19

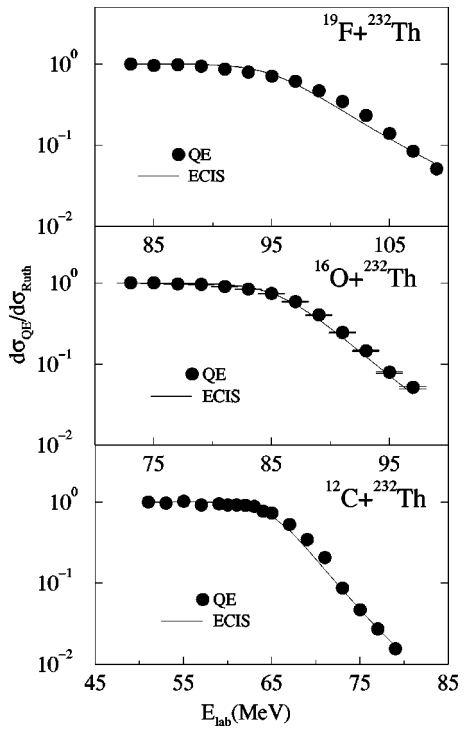

FIG. 7. The measured QE excitation function at $\theta_{lab}=170°$ for ^{12}C, ^{16}O, and ^{19}F+^{232}Th reactions. The continuous line is the predictions of ECIS for the potential parameters listed in Table I.

shows reasonable agreement with the prediction of coupled channel fusion model (CCDEF) calculations as well as with the barrier distributions obtained from fusion excitation function [5]. We have compared the fusion spin distributions obtained from quasielastic excitation functions with that obtained from fission fragment angular distributions in these heavy fissile systems.

The measured quasielastic excitation function at $\theta_{lab}=170°$ has been fitted with the optical model code ECIS [16] to obtain potential parameters which give the best fit to the experimental data as shown in Fig. 7. The wide range of bombarding energies covered in this study allowed us to investigate the global behavior of the optical model parameters. The potential parameters so obtained for all the three systems ^{12}C, ^{16}O, and ^{19}F+^{232}Th reactions are listed in Table I. The values of V_0, R_0, a_0, R_{0i}, and a_{0i} were kept same for the three systems and only the depth of the imaginary potential W_0 was varied to fit the excitation functions. It is seen that the depth of the imaginary potential generally increases with mass of the projectile. In the case of ^{19}F a somewhat larger value of the imaginary potential as compared to the other two nuclei, was needed to fit the quasielastic excitation function. This may indicate that in this reaction a large number of channels are opening up aiding the fusion process and thereby depleting the strength from the quasielastic excitation function. To include it theoretically one needs a higher value of imaginary potential. The reaction cross sections and partial wave distributions obtained with the tabulated potential parameters are identified as for the fusion channel. The $\langle l^2 \rangle$ was then obtained from the partial waves leading to fusion as outlined in Ref. [17].

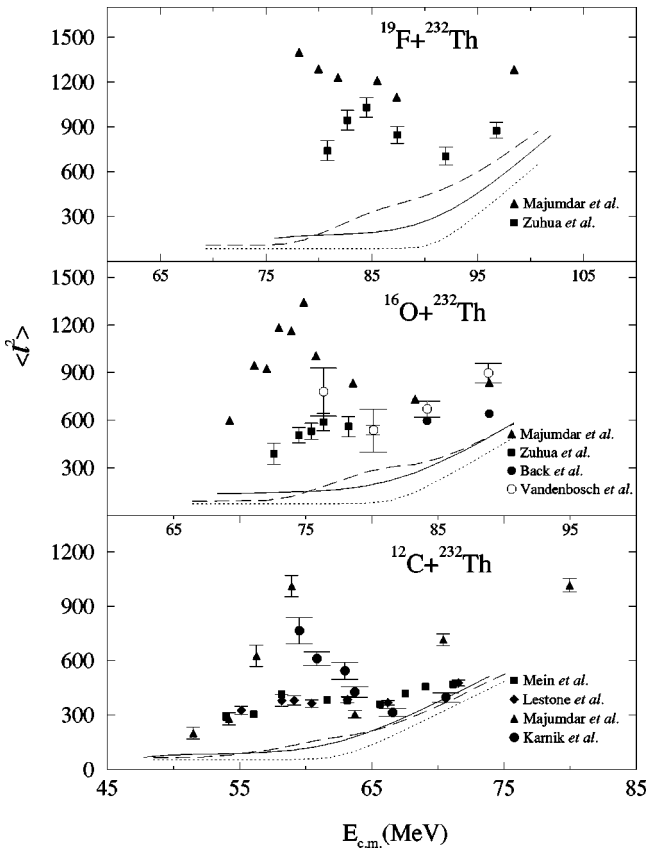

FIG. 8. The dependence of $\langle l^2 \rangle$ values as a function of bombarding energy calculated from QE data are shown by solid line. Also shown in the figure are the predictions of CCDEF without coupling (dotted lines) and with coupling (dashed lines) along with that obtained from fission fragment anisotropy measurements of Refs. [18–24] for ^{12}C, ^{16}O, and ^{19}F+^{232}Th reactions.

The dependence of $\langle l^2 \rangle$ values as a function of bombarding energy for all the three systems are shown in Fig. 8. The $\langle l^2 \rangle$ values obtained from the analysis of the quasielastic scattering data and from the CCDEF code along with that obtained from fission fragment measurements of Refs. [18–24] are shown in Fig. 8. It is seen that the $\langle l^2 \rangle$ values obtained from QE data and that from standard fusion model CCDEF are quite similar for all the three systems. The $\langle l^2 \rangle$ values derived from the fission fragment angular anisotropies using SSPM calculations are in complete disagreement with those obtained from the QE data and the CCDEF calculations for all the three systems, especially at sub-barrier energies. As mentioned in Ref. [5] it implies that the formalism employed to derive $\langle l^2 \rangle$ in the sub-barrier region is not justified, as the K_0^2 parameter may be modified if other modes of fission [25] such as preequilibrium or quasifission [26] dominate in this region. Some recent studies [27] show that the fission **K** distribution may be altered due to the coupling with the entrance channel **K** distribution arising from the deformation of the target nucleus.

IV. TRANSFER CROSS SECTIONS AND TRANSFER PROBABILITIES

The differential transfer cross-section data measured for the reactions ^{16}O+^{232}Th and ^{19}F+^{232}Th as a function of

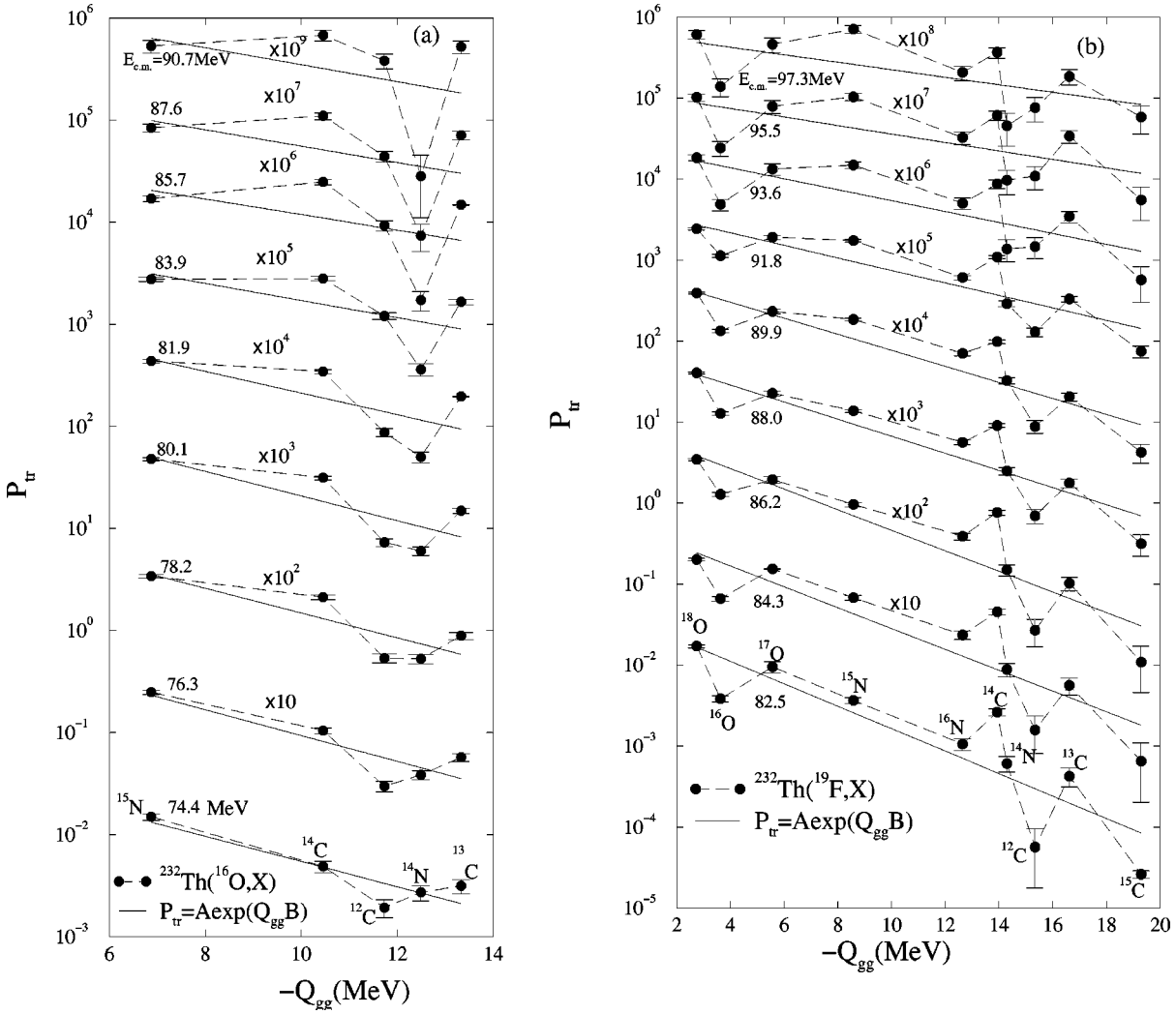

FIG. 9. (a) Variation of transfer probability $P_{\rm tr}$ as a function of the ground state Q value $(-Q_{gg})$ for ^{16}O+^{232}Th system. The solid lines are the exponential fit to the data. (b) Variation of transfer probability $P_{\rm tr}$ as a function of the ground state Q value $(-Q_{gg})$ for ^{19}F +^{232}Th system. The solid lines are the exponential fit to the data.

bombarding energy at the fixed backward angle of $\theta=170°$ have been shown in Figs. 5(a) and 5(b). The cross-section data have been shown as the ratio to the Rutherford scattering cross section at each energy, which corresponds to the transfer probability for each transfer channel ($P_{\rm tr}=d\sigma_{\rm tr}/d\sigma_{\rm Ruth}$). It is seen from the Figs. 5(a) and 5(b) that the transfer probability for backward emission of the ejectiles is maximum around Coulomb barrier energies. Transfer is hindered at energies much below the barrier because the distance of closest approach becomes large, leading to decrease in the nuclear overlap. At above barrier energies, the increased overlap results in more dissipative collisions which finally results in fusion. Since the transfer probability, $P_{\rm tr}$ for a given transfer channel is known to depend strongly on the ground state Q value (Q_{gg}) of the reaction we have studied the variation of the observed $P_{\rm tr}$ with respect to the ground state Q value of the reaction. Figures 9(a) and 9(b) show the variation of $P_{\rm tr}$ with the Q_{gg} in ^{16}O+^{232}Th and ^{19}F+^{232}Th reactions at different bombarding energies. The dominant cross sections in the ^{19}F+^{232}Th reaction are the transfer channels of ^{18}O$(1p)$, ^{17}O$(1p1n)$, ^{15}N(1α), ^{14}C$(1\alpha1p)$. In the case of ^{16}O+^{232}Th reaction, the dominant channels are ^{15}N$(1p)$, ^{14}C$(2p)$, and ^{13}C$(2p1n)$. It is seen that in both the systems, there is a general decrease in $P_{\rm tr}$ with increasing negativity of the ground state Q value for the transfer channels. The $P_{\rm tr}$ data were fitted with an exponential function of the form $P_{\rm tr}=A\exp(Q_{gg}B)$ as shown by the solid lines. The slope of the exponential shows a systematic variation with increasing bombarding energy ranging from about 3.5 to 5.2 MeV^{-1} in ^{16}O and 3.1 to 8.3 MeV^{-1} in ^{19}F. At lower bombarding energies, there is much stronger variation of $P_{\rm tr}$ with the Q value, which is expected on the basis of the energetics of the reaction. One can also see from Figs. 9(a) and 9(b) that there are systematic deviations from the smooth exponential behavior for certain transfer channels, which may be connected to the internal structure of the projectile. For the ^{16}O projectile, as the bombarding energy increases, the ^{14}C channel corresponding to $2p$ transfer shows a large enhancement, whereas the ^{14}N channel corresponding to the $1p1n$ transfer has a large suppression. The

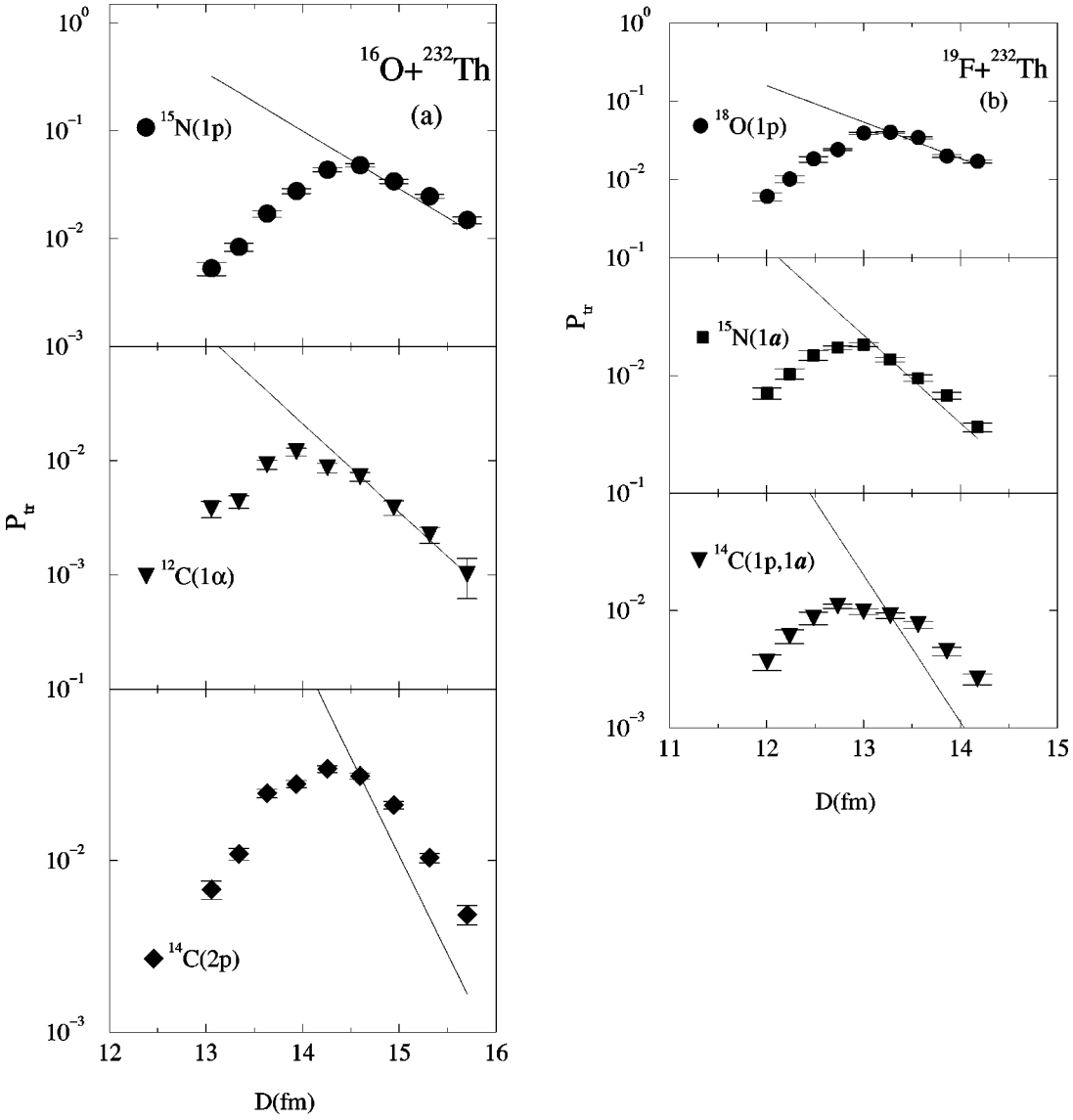

FIG. 10. (a) Variation of transfer probability (P_{tr}) as a function of distance of closest approach for various transfer channels observed in $^{16}O+^{232}Th$ reaction. The solid lines have slopes corresponding to binding-energy-derived decay constants for various transfer channels. (b) Variation of transfer probability as a function of distance of closest approach for transfer channels observed in $^{19}F+^{232}Th$ reaction. The solid lines have slopes corresponding to binding-energy-derived decay constants for various transfer channels.

1α-transfer channel corresponding to ^{12}C also shows a slightly increasing strength as the bombarding energy is increased. In case of ^{19}F projectile [Fig. 9(b)], there is large enhancement in the ^{15}N channel corresponding to 1α transfer, as the bombarding energy increases. The ^{14}C channel corresponding to $(1\alpha 1p)$ transfer is seen to be enhanced at all bombarding energies. One also sees that the $^{16}O(1p2n)$ transfer and $^{15}C(3p1n)$ transfer channels are suppressed in the $^{19}F+^{232}Th$ reaction at all energies. The large enhancement in certain transfer channels are possibly due to simultaneous cluster or multinucleon transfers from the projectile to the target nucleus, as facilitated by their internal structures.

Inspite of considerable progress in the understanding of transfer reactions, the complex problem of multinucleon transfer has not yet been adequately understood and therefore, much of the nuclear structure information extracted so far from the data is still of qualitative nature. A large amount of work has been reported [28–32] on four nucleon or α-particle transfer in order to establish the mechanism of the transfer process and to test the relevant nuclear structure models involving α clustering in nuclei. The present study has provided further experimental inputs to investigate in detail the mechanism of simultaneous and correlated transfer of particles and to study the clusterization aspects in heavy ion induced reactions. The possibility of simultaneous correlated transfers of (αp), $(\alpha p,\alpha)$, and (3α) from the ^{19}F projectile on to the target ^{232}Th were also reported earlier [29].

The present measurements at below barrier energies also provide an alternate way to study the ''slope anomaly'' in transfer reactions. The present measurements on the variation

TABLE II. Experimental decay constants obtained from an exponential fit to the measured transfer probability and also listed are decay constants calculated on the basis of the binding energy.

System	Channel	α_{calc}	α_{expt}
$^{19}F+^{232}Th$	^{18}O	0.53	0.54 ± 0.09
	^{15}N	0.86	0.75 ± 0.07
	^{14}C	$\alpha_{p,\alpha}=1.44$	0.74 ± 0.10
$^{16}O+^{232}Th$	^{15}N	0.60	0.54 ± 0.03
	^{14}C	$\alpha_{2p}=1.17$	0.89 ± 0.07
	^{12}C	0.99	0.75 ± 0.11

of P_{tr} as a function of D for various transfer channels have been shown in Figs. 10(a) and 10(b) for the $^{16}O+^{232}Th$ and $^{19}F+^{232}Th$ reactions. The data at higher D values were fitted by an exponential function to get the slope parameters. The comparison of slope parameters α_{calc} derived from binding-energy based decay constant to that of experimental slope parameters α_{expt} is given in Table II. It is seen that in the case of both ^{16}O, $^{19}F+^{232}Th$ induced reactions, the experimental slope parameters α_{expt} for $1p$ and 1α transfer show good agreement with the calculated values of α_{calc}. However, for more complex transfers of $2p$ or $1\alpha 1p$ transfers, the experimental slope parameters do not agree with calculated values. This is also shown graphically in Figs. 10(a) and 10(b) by the solid lines corresponding to the calculated slope parameters. It may be concluded that the semiclassical picture, is valid for one step transfer of nucleons or clusters and it breaks down while considering multistep or complex multinucleon transfers in the transfer reactions.

V. SUMMARY AND CONCLUSIONS

In the present work, we have studied the fusion barrier distributions and spin distributions in ^{16}O, $^{19}F+^{232}Th$ reactions from the measurement of the quasielastic excitation functions at backward angle of $\theta_{lab}=170°$ at above and below the fusion barrier. The representation of the fusion barrier distributions extracted from the present measurements agree well with the calculations based on the CCDEF fusion model. The quasielastic scattering data have, therefore, provided a useful method to extract fusion barrier distributions for the heavy fissile systems. The compound nuclear mean square spin $\langle l^2\rangle$ derived from QE measurements also agree with the results from standard fusion model CCDEF but are in complete disagreement with those obtained from fission fragment angular distribution based on the standard saddle point model calculations. The present measurements on the cross sections of different transfer channels in the reactions of ^{16}O, $^{19}F+^{232}Th$ at energies around Coulomb barrier have been analyzed to derive the transfer probabilities. The transfer probabilities, show an exponential decrease with the ground state Q_{gg} value of the various transfer channels. However, for certain transfer channels strong variation in P_{tr} versus ground state Q_{gg} value for different bombarding energies was observed, which may be connected with the internal structure of the projectile. In case of $^{16}O+^{233}Th$ reaction, $2p$ stripping corresponding to ^{14}C shows a large enhancement in comparison to $1p1n$ stripping in ^{14}N channel which has a large suppression. The 1α transfer corresponding to ^{12}C channel shows a slight increasing strength as the bombarding energy is increased. In case of $^{19}F+^{232}Th$ reaction the 1α transfer corresponding to ^{15}N channel shows large enhancement whereas certain other channels such as $^{16}O(1p2n)$ and $^{15}C(3p1n)$ transfers are suppressed. The large enhancement in $2p$ transfer channel in ^{16}O induced reaction and 1α transfer in ^{19}F induced reaction point out to the possibility of simultaneous cluster or multinucleon transfers as facilitated by their internal structures. The present data were also analyzed to obtain the variation of the transfer probabilities as a function of the distance of closest approach (D) for both the systems. The experimental slope parameters obtained from the plot of P_{tr} versus D plot were compared with semiclassical calculations. It is observed that the semiclassical picture is valid for $1p$, 1α transfer around Coulomb barrier energies. However, for more complex channels of $2p$ and $1p1\alpha$ transfers, the slope anomaly exists between the experimental and calculated values. These studies have provided new insight into the mechanism of transfer reactions involving multinucleon and cluster transfers in the heavy ion collisions at near and below Coulomb barrier energies.

ACKNOWLEDGMENTS

The authors would like to thank Dr. S. S. Kapoor for many helpful discussions and suggestions on this work. We would also like to thank Dr. B. K. Jain for his interest and encouragement. Thanks are also due to Pelletron staff for their help with the accelerator operations. Two of us (S.S. and R.V.) would like to acknowledge the support of Board for Research in Nuclear Science (BRNS), DAE, and Department of Science and Technology, Government of India for providing funds for this work.

[1] M. Beckerman, Rep. Prog. Phys. **51**, 1047 (1988).
[2] S. G. Steadman and M. J. Rhoades-Brown, Annu. Rev. Nucl. Part. Sci. **36**, 649 (1986).
[3] N. Rowley, G. H. Satchler, and P. H. Stelson, Phys. Lett. B **254**, 25 (1991).
[4] H. Timmers, J. R. Leigh, M. Dasgupta, D. J. Hinde, R. C. Lemmon, J. C. Mein, C. R. Morton, J. O. Newton, and N. Rowley, Nucl. Phys. **A584**, 190 (1995).
[5] R. Varma, Shrabani Sinha, B. K. Nayak, R. G. Thomas, A. Saxena, D. C. Biswas, L. M. Pant, D. M. Nadkarni, R. K. Choudhury, and P. Bhattacharya, Phys. Rev. C **57**, 3462 (1998).
[6] V. V. Volkov, G. F. Gridnev, G. N. Zorin, and L. P. Chelnokov, Nucl. Phys. **A126**, 1 (1969).
[7] P. Christensen, V. I. Manko, F. D. Becchetti, and R. J. Nickles, Nucl. Phys. **A207**, 33 (1973).

[8] R. Bass, *Nuclear Reactions with Heavy Ions* (Springer, Berlin, 1980).
[9] L. Corradi, S. J. Skorka, U. Lenz, K. E. G. Lobner, P. R. Pascholat, U. Quade, K. Rudolph, W. Schomburg, M. Steinmayer, H. G. Thies, G. Montagnoli, D. R. Napoli, A. M. Stefanini, A. Tiveli, S. Beghini, F. Scarlassara, C. Signorini, and F. Soramel, Z. Phys. A **335**, 55 (1990).
[10] A. H. Wuosmaa *et al.*, Phys. Lett. B **255**, 316 (1991).
[11] C. V. K. Baba *et al.*, Phys. Lett. B **338**, 147 (1994).
[12] Fred S. Goulding and Bernard G. Harvey, Annu. Rev. Nucl. Part. Sci. **25**, 167 (1975).
[13] J. Fernandez-Niello, C. H. Dasso, and S. Landowne, Comput. Phys. Commun. **54**, 409 (1989).
[14] N. Majumdar, P. Bhattacharya, D. C. Biswas, R. K. Choudhury, D. M. Nadkarni, and A. Saxena, Phys. Rev. Lett. **77**, 5027 (1996).
[15] M. Dasgupta, D. J. Hinde, N. Rowley, and A. M. Stefanini, Annu. Rev. Nucl. Part. Sci. **48**, 401 (1998).
[16] J. Raynal, *Computing as Language of Physics* (IAEA, Vienna, 1972), p. 281.
[17] S. V. S. Sastry, S. K. Kataria, A. K. Mohanty, and I. J. Thompson, Phys. Rev. C **54**, 3286 (1996).
[18] R. Vandenbosch, T. Murakami, C. C. Sahm, D. D. Leach, A. Ray, and M. J. Murphy, Phys. Rev. Lett. **56**, 1234 (1986).
[19] B. Back *et al.*, Phys. Rev. C **33**, 385 (1986).
[20] N. Majumdar, P. Bhattacharya, D. C. Biswas, R. K. Choudhury, D. M. Nadkarni, and A. Saxena, Phys. Rev. C **53**, R544 (1996).
[21] A. Karnik, S. Kailash, A. Chatterjee, P. Singh, A. Navin, D. C. Biswas, D. M. Nadkarni, A. Shrivastava, and S. S. Kapoor, Z. Phys. A **351**, 195 (1995).
[22] J. P. Lestone, A. A. Sonzogni, M. P. Kelly, and D. Prindle, Phys. Rev. C **55**, R16 (1997).
[23] J. C. Mein, D. J. Hinde, M. Dasgupta, J. R. Leigh, J. O. Newton, and H. Timmers, Phys. Rev. C **55**, R995 (1997).
[24] Zuhua Liu, Huanqiao Zhang, Jincheng Xu, Yu Qiao, Xing Qian, and Chengjian Lin, Phys. Lett. B **353**, 173 (1995).
[25] V. S. Ramamurthy, S. S. Kapoor, R. K. Choudhury, A. Saxena, D. M. Nadkarni, A. K. Mohanty, B. K. Nayak, S. V. Sastry, S. Kailas, A. Chatterjee, P. Singh, and A. Navin, Phys. Rev. Lett. **65**, 25 (1990).
[26] D. J. Hinde, M. Dasgupta, J. R. Leigh, J. P. Lestone, J. C. Mein, C. R. Morton, J. O. Newton, and H. Timmers, Phys. Rev. Lett. **74**, 1295 (1995).
[27] D. Vorapic and B. Ivanisevic, Phys. Rev. C **52**, 1980 (1995).
[28] L. Corradi, A. M. Stefanini, D. Ackermann, S. Beghini, G. Montagnoli, C. Petrache, F. Scarlassara, C. H. Dasso, G. Pollarolo, and A. Winter, Phys. Rev. C **49**, R2875 (1994).
[29] D. C. Biswas, R. K. Choudhury, D. M. Nadkarni, and V. S. Ramamurthy, Phys. Rev. C **52**, R2827 (1995).
[30] L. Jarczyk, B. Kamys, M. Kistryn, A. Magiera, Z. Rudy, A. Strzalkowski, R. Barna, V. D'Amico, D. De. Pasquale, A. Italiano, and M. Licandro, Phys. Rev. C **54**, 1302 (1996).
[31] D. C. Biswas, R. K. Choudhury, B. K. Nayak, D. M. Nadkarni, and V. S. Ramamurthy, Phys. Rev. C **56**, 1 (1997).
[32] C. L. Jiang, K. E. Rehm, H. Esbensen, D. J. Blumenthal, B. Crowell, J. Gehring, B. Glagola, and J. P. Schiffer, Phys. Rev. C **57**, 2393 (1998).